

# Gradient Magnesium Content Affects Nanomechanics via Decreasing the Size and Crystallinity of Nanoparticles of Pseudoosteodentine of the Pacific Cutlassfish, *Trichiurus lepturus* Teeth

Li Tang, Yongfeng Li, Ruiqi Li, Xingfu Tao, and Xiaofeng Huang\*

Cite This: *ACS Omega* 2022, 7, 39214–39223

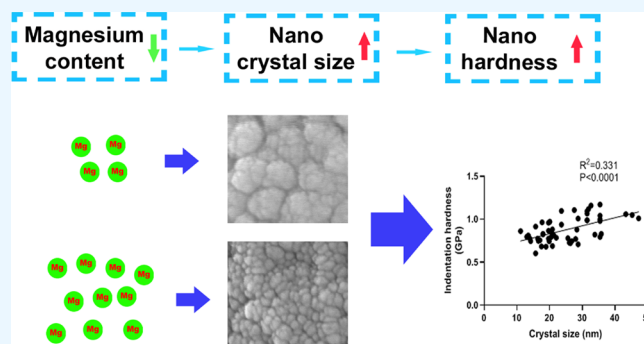
Read Online

ACCESS |

Metrics & More

Article Recommendations

**ABSTRACT:** The formation of biomaterials such as enamel, dentin, and bone is important for many organisms, and the mechanical properties of biomaterials are affected by a wide range of structural and chemical factors. Special dentins exist in extant aquatic gnathostomes, and many more are present in fossils. When a layer of compact orthodentine surrounds the porous osteodentine core in the crown, the composite dentin is called pseudoosteodentine. Using various high-resolution analytical techniques, including micro-computed tomography (micro-CT), scanning electron microscopy (SEM), energy-dispersive X-ray spectroscopy (EDS), Raman spectroscopy, and nanoindentation, we analyzed the micro- and nanostructures, chemical composition, and mechanical properties of pseudoosteodentine in the Pacific cutlassfish, *Trichiurus lepturus* teeth. Nanoscale oval-shaped hydroxyapatite (HA) crystals were distributed in a disordered manner in the pseudoosteodentine, and a cross-sectional analysis showed that the mineral crystallinity and crystalline particle size of the outer orthodentine were greater than those of middle and inner osteodentine. Moreover, the outer orthodentine comprised a mixture of smaller crystals and larger, more mature crystals. The nano-hardness and nano-stiffness of outer orthodentine were significantly higher than those of middle and inner osteodentine along a radial direction. The hardness and stiffness of pseudoosteodentine were inversely proportional to its magnesium (Mg) content. These data are consistent with the concept that Mg delays crystal maturation. The crystal size, crystallinity, nano-hardness, and nano-stiffness of pseudoosteodentine all decreased commensurately with the increase of its Mg concentration. The pseudoosteodentine of *T. lepturus* also can be regarded as a functional gradient material (FGM) because its mechanical properties are closely related to its chemical composition and nanostructure. Special pseudoosteodentine may therefore serve as a design standard for biomimetic synthetic mineral composites.



## 1. INTRODUCTION

As highly calcified organs, teeth are important for predation and chewing.<sup>1,2</sup> A tooth generally contains three mineralized structures: enamel, dentin, and cementum.<sup>3</sup> Although the chemophysical properties of enamel, dentin, and bone are well known,<sup>4–6</sup> few works have studied the microstructure and hardness of rare dentin type-pseudoosteodentine.<sup>7</sup> Dentin maintains the bulk and shape of teeth, supports enamel, and connects to the jaw bone,<sup>8</sup> suggesting that its strength determines that of the tooth to a great extent. Therefore, it is important to understand the physical and chemical properties of dentin, especially in slender teeth where the dentin is more likely to be broken.

Chemical compositions alter the biomineralization of teeth. The crystal size of minerals affects its mechanical strength. Boskey proposed that the crystal size and perfection of bone

minerals affect the ability of the bone composite to respond to load.<sup>9</sup> However, it is not unambiguously clear how the crystal size affects the properties of mineralized materials. Hydroxyapatite (HA) is the main mineral phase of bone and teeth and contains several ionic substitutions, such as  $\text{CO}_3^{2-}$ ,  $\text{F}^-$ ,  $\text{Mg}^{2+}$ , and  $\text{Na}^+$ , that change its structure, stability, as well as mechanical properties.<sup>10,11</sup> Magnesium is an important trace element in bone and teeth and plays a key role in bone metabolism,<sup>12</sup> the mechanical properties of enamel,<sup>13</sup> and

Received: August 16, 2022  
Accepted: October 13, 2022  
Published: October 23, 2022



development of dental caries.<sup>14</sup> Kis et al.<sup>13</sup> found that increasing experimentally the  $Mg^{2+}$  concentration in the surface enamel of human primary teeth resulted in a notable increase in its nano-hardness. On the contrary, Cuy et al. found that the  $Mg^{2+}$  concentration in the enamel of human permanent teeth was lower on the surface than inside and was inversely proportional to the hardness of the enamel.<sup>15</sup> Therefore, the relationship between the  $Mg^{2+}$  concentration and enamel hardness remains to be understood.

Our previous work identified two types of dentin in *Trichiurus lepturus* teeth and showed that there were marked differences between both their forming cell morphologies and organic matrix scaffolds.<sup>16</sup> Dentin is a hierarchical, nano-structured, biological composite formed by matrix-mediated biomineralization and whose cellular components control the mineral deposition.<sup>17</sup> Differences between the mineralized deposited substrates within the two types of dentin are likely responsible for their differences in their mechanical properties. The purpose of this study was to characterize special dentin of *T. lepturus*. Scanning electron microscopy (SEM), energy-dispersive X-ray spectroscopy (EDS), micro-computed tomography (micro-CT), Raman spectroscopy, and nanoindentation were used to compare the chemical compositions, nanocrystalline structures, and mechanical properties of different types of dentins so as to understand the relationships of constituent/structure–property and further guide the development of clinical restorative materials.

## 2. MATERIALS AND METHODS

**2.1. Samples.** Ten adult specimens of the Pacific cutlassfish, *Trichiurus lepturus* (total length, 84~92 cm), were purchased from commercial fisheries already deceased and transported to the laboratory on ice in China. The upper jaw of each specimen was dissected and then removed the soft tissues around the functional teeth and attached to the jaw before micro-CT. Fifteen functional premaxillary teeth of *T. lepturus* were freed from the upper jaw using dental hand set, washed, and cleaned in Hanks' balanced salt solution (14175095, Gibco, USA). The upper jaws and teeth of *T. lepturus* were fixed in 10% neutral buffered formalin solution for 1 day and then dehydrated in a series of solutions with ascending ethanol concentration (25, 50, 75, 85, 95, and 100% v/v), stayed for 30 min at each concentration, treated with 100% ethanol three times, and dried at room temperature.

**2.2. Sample Preparation.** The premaxillary teeth of *T. lepturus* were embedded in a cold-curing epoxy resin (PS-M01, Pengsheng, China) and allowed to polymerize overnight at room temperature. A water-cooled, slow speed diamond saw (STX-202A, SFMIT, China) was utilized to cut each resin-embedded tooth in two halves at the middle of the tooth and perpendicular to the long axis of the tooth to generate transverse surfaces. When a correlation between mechanical properties and composition was examined, one half of a tooth was used for nanoindentation measurements and the other half for X-ray energy-dispersive spectrometer, Raman spectroscopy. The transverse surfaces were ground using a series of Buehler silicon carbide disks with descending grain sizes (from P1200 to P10000) on a polishing machine (MetaServ 250, Buehler, USA). Finally, ground samples were polished using suspensions of diamond particles and gamma alumina powder (3, 1, and 0.05  $\mu\text{m}$ ; Buehler, USA) on a velvet disk for 9 min in total. Samples were rinsed with distilled water, cleaned for 5 min

using an ultrasonicator to remove polishing powder, and then air-dried.

Three transverse-fractured tooth surfaces of *T. lepturus* were created by applying careful hammer strokes to the back of a new, sharp blade placed midway along the length of the tooth.

To reveal microstructural patterns of the dentin in the teeth of *T. lepturus*, two polished, epoxy-embedded samples were superficially etched by immersion in 3.7% w/w HCl for 10 s at room temperature.

**2.3. Micro-Computed Tomography.** One upper jaw and tooth of *T. lepturus* were scanned using a computed tomography (CT) imaging system (SkyScan1276, Bruker, Belgium). The X-ray source parameters were set to 70 keV, 200  $\mu\text{A}$ , and a voxel size of 10  $\mu\text{m}$  for the upper jaw and 5  $\mu\text{m}$  for the tooth. Other parameters were as follows: scanner model = step and shoot, step size = 0.2°, projections = 1028, exposure time = 1300 ms, angular range = 205.6°, filter = Al (0.25 mm thickness), and reconstruction program = NRecon v1.7.4.2. Image stacks were combined using the CT Vox software (v3.3.0.0, Bruker, Kontich, Belgium) to visualize a three-dimensional model. Virtual color indicated variations in the mineral density, such that sites with a low mineral content were shown in deep yellow while sites with a high mineral content were shown in white and pale yellow.

**2.4. Scanning Electron Microscopy (SEM) and EDS Characterization.** The transversely polished sections, the fractured fragments as well as the etched cross section of *T. lepturus* were examined using a scanning electron microscope with a secondary electron detector at an accelerating voltage of 15~20 kV in high vacuum mode (S-4800, HITACHI, Japan) after being coated with a thin layer of gold. Three transversely fractured teeth were chosen to image crystals of the interest regions from outer dentin to inner dentin. The outermost orthodentine was assigned as the outer layer, and the osteodentine covered by orthodentine was divided into a middle layer and an inner layer. To calculate the crystalline particles' sizes, the diameter of 20 particles from each SEM picture was measured with Image J analysis software.

For elemental analysis of dentin of *T. lepturus*, five polished samples were probed using an EMAX-350 energy-dispersive X-ray analyzer equipped with a silicon drift detector (127 eV, 40  $\text{mm}^2$ ) under accelerating voltage of 15 kV, a spot size of 4, an acquisition time of 5 min for mapping, and 1 min for a point analysis. Elemental mappings provided images of the spatial distribution of elements on the cross-sectional surface. The semi-quantitative elemental content of three dentin layers in five transverse sections was obtained and analyzed using Genesis EDS microanalysis software (EDAX Inc., NJ, USA). It should be noted that the carbon (C) intensity was the total intensity of C from organic components and  $\text{CO}_3^{2-}$  in apatite. Therefore, the net carbon intensity caused by organic components was lower than the obtained value, which was difficult to evaluate.

**2.5. Raman Spectroscopy.** To clarify the mineral phase and crystallinity of the dentin of *T. lepturus*, Raman analyses were carried out using an inVia Qontor confocal Raman microscope (Renishaw plc, Gloucestershire, UK). The Raman spectrometer was equipped with a 785 nm, 300 mW excitation laser and a DM4000 microscope (Leica Microsystems).

Using the embedded, polished sections from three different teeth, for each dentin region (outer, middle, and inner), three spectra were acquired (from 200 to 3200  $\text{cm}^{-1}$ ) by focusing the laser beam through a 50 $\times$  - water immersion objective lens

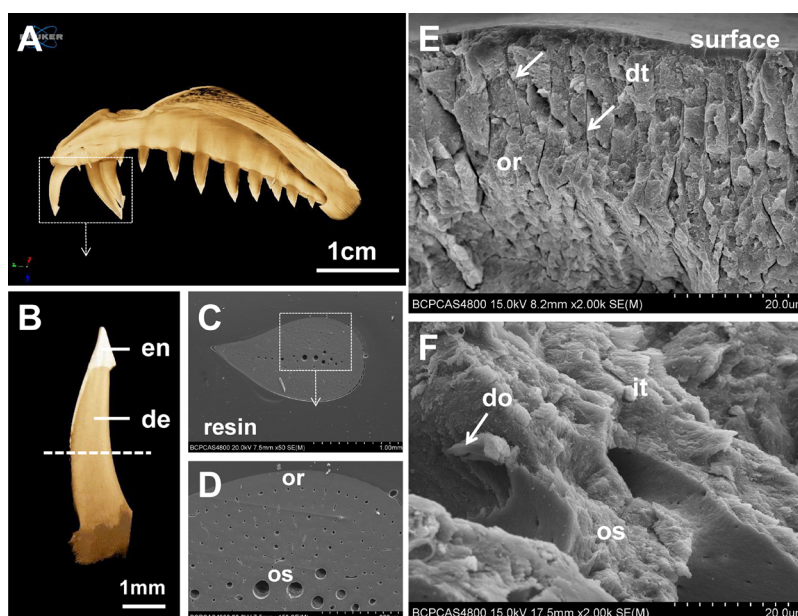


**Figure 1.** Tissue structure of dentin (pseudoosteodentine) of *Trichiurus lepturus*. (A) 3D reconstruction image of an upper jaw of *T. lepturus*. Large teeth are examined in this study indicated by a rectangular box. (B) 3D reconstruction image of a functional premaxillary tooth. Dentin makes up most of the tooth and overlain little by a hypermineralized enameloid. The white dotted line indicates the detection location. (C) SEM image of the polished transverse section of a premaxillary tooth. Instead of a pulp cavity, a tooth is replaced by a porous osteodontine (os). (D) Larger view of the boxed area in C. Osteodontine is covered by a thin layer of compact hard tissue. (E) Outer orthodontine layer of a transversely fractured tooth contains parallel dentinal tubules, which is a typical characteristic of orthodontine. (F) Inner osteodontine layer of a transversely fractured tooth resembles bone. Dentinal tubules radiate from the dentinal osteons. en, enameloid; de, dentin; or, orthodontine; os, osteodontine; do, dentinal osteons; dt, dentinal tubule; and it, interosteonal tissue.

and 10 s exposure onto the tooth sections. A grating with 1200 grooves/mm produced a resolution of  $2\sim 4\text{ cm}^{-1}$ . Raman images were collected using an inVia Qontor confocal Raman microscope with a Centrus CCD detector (Renishaw), which allowed for spectral acquisitions of 1 ms and was free of ripple effects in the near infrared region. Images were acquired using StreamLine (Renishaw) fast imaging. To analyze the spectral information, the obtained Raman spectrum was smoothed and artificially multipoint baseline corrected. Furthermore, the full width at half maximum (FWHM) of the  $\nu_1\text{ PO}_4^{3-}$  band near  $960\text{ cm}^{-1}$  was calculated to determine the dentin crystallinity.<sup>18</sup> The areas of amide I and  $\nu_1\text{ PO}_4^{3-}$  were used to evaluate the contents of organic and inorganic substances in apatite, respectively. The Origin 8.6 software (OriginLab, Massachusetts, USA) was used for data analysis.

**2.6. Nanoindentation.** Five polished transverse sections of dentin of *T. lepturus* was similarly divided into outer orthodontine, middle osteodontine, and inner osteodontine layers. Nanoindentation experiments were conducted using a UNHT S/N instrument (Anton Paar, Austria) with a diamond Berkovich tip (radius = 100 nm). Twenty indentations of each layer with a maximum load of 2.5 mN were made to determine the positional dependence of its mechanical properties. Specimens were indented at a loading and unloading rate of 5 mN/min. The typical indentation depth was approximate 280 nm and a minimum distance of  $10\text{ }\mu\text{m}$  was maintained between adjacent indentations to prevent coupling effects. The load was continuously recorded as a function of displacement throughout testing. Data were analyzed using standard routines (Oliver & Pharr, 1992) to determine the nano-hardness and nano-stiffness.<sup>19</sup>

**2.7. Statistical Analysis.** For quantitative data obtained from crystalline particle size, EDS point elemental analysis, and

nanoindentation, significant differences among groups were determined using one-way analysis of variance, followed by Tukey's multiple-comparison test; alternatively, when data were not normally distributed, the Kruskal–Wallis test was used, followed by Dunn's multiple-comparison test. Pairwise correlations among Mg content, crystalline particle size, hardness, and stiffness of the dentin were determined using Pearson's correlation coefficient. To establish correlations between the crystalline particle size and nanoproperties (hardness and stiffness) as well as Mg content (wt %), we selected two teeth from the same fish, one tooth for crystal size and one tooth for nanoproperties and chemical elements. For each pair, the correlation coefficient ( $r$ ), coefficient of determination ( $r^2$ ), and significance of the correlation ( $p$ ) were calculated. Statistical significance was defined as  $p < 0.05$ . All statistical analyses were conducted using Prism v8.0 (Graph Pad Software, California, USA) software.

### 3. RESULTS

**3.1. Histological Structure and Classification of *Trichiurus lepturus* Dentin.** This study examined large, slender teeth that were ankylosed in the front of the premaxilla (Figure 1A). Micro-CT imaging showed that deep yellow-colored dentin had a lower density than the white enameloid, which covered only the tip and part of the cutting edge of the tooth (Figure 1B). Thus, dentin occupied the bulk of the tooth volume (Figure 1B). Figure 1C showed the arrangement of orthodontine and osteodontine that replaced the pulp cavity. There was no clear demarcation between orthodontine and osteodontine, which could only be distinguished by morphology. Orthodontine was recognizable near the surface of the tooth by its parallel tubules, which were much smaller than the dentinal osteons of the osteodontine in the tooth interior

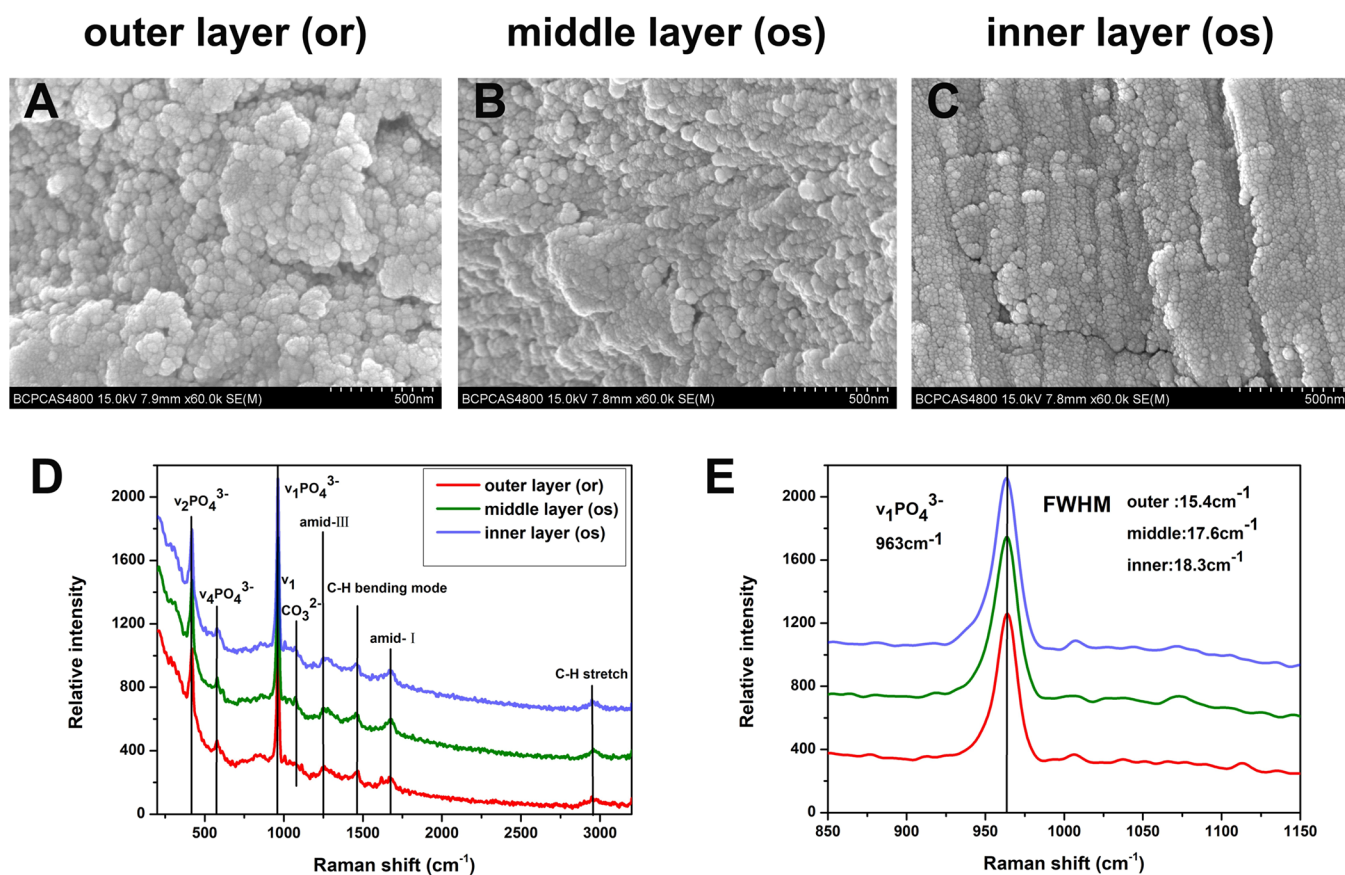


**Figure 2.** Crystalline particle size, crystallinity, and composition of pseudoosteodentine of *Trichiurus lepturus*. (A) Nanoparticles of outer orthodontine layer from a transversely fractured tooth (diameter:  $33.84 \pm 6.15$  nm). (B) Nanoparticles of middle osteodentine layer from a transversely fractured tooth (diameter:  $21.87 \pm 4.03$  nm). (C) Nanoparticles of inner osteodentine layer from a transversely fractured tooth (diameter:  $16.55 \pm 3.54$  nm). (D) Raman spectra of pseudoosteodentine assigned to hydroxyapatite (HA). (E) The full width at half maximum (FWHM) of the  $\nu_1$   $\text{PO}_4^{3-}$  band showing the crystallinity of pseudoosteodentine gradually decreases from outside to inside. Avoid overlap by shifting the spectrum. or, orthodontine; and os, osteodentine.

(Figure 1E,F). Tubules in the orthodontine typically measured approximately  $0.16 \mu\text{m}$  in diameter (Figure 1E). Osteodentine was composed of dentinal osteons and interosteonal tissue (Figure 1F). These canals were  $10\sim 65 \mu\text{m}$  in diameter. The identification of both orthodontine and osteodentine showed that the teeth of *T. lepturus* had a special pseudoosteodont histotype (Figure 1C,D).

**3.2. Crystal Properties of Pseudoosteodentine of *Trichiurus lepturus*.** The high-resolution SEM images of pseudoosteodentine in the teeth of *T. lepturus* at different layers were shown in Figure 2. Elliptical crystalline nanoparticles were randomly arranged in the total thickness of pseudoosteodentine. Although they were similar in shape, they differed greatly in size (Figure 2A–C). The outer orthodontine layer consisted of larger, oval-shaped composite crystals ( $33.84 \pm 6.15$  nm in diameter). Many small crystals were adhered to the composite crystals, yielding a broad crystal size distribution (Figure 2A). The middle osteodentine layer contained fewer composite crystals than the outer orthodontine, and the crystal sizes were smaller ( $21.87 \pm 4.03$  nm in diameter) and more uniform in term of size (Figure 2B). Large composite particles were almost absent from the inner osteodentine layer, which was instead composed of predominantly small, even crystals ( $16.55 \pm 3.54$  nm in diameter) (Figure 2C).

Raman spectroscopy analysis showed characteristic features of pseudoosteodentine (orthodontine + osteodentine) similar

to carbonated HA, like mammal dentin, enamel, and bone<sup>18,20,21</sup> (Figure 2D). The  $\nu_1$   $\text{PO}_4^{3-}$  ( $963 \text{ cm}^{-1}$ ),  $\nu_2$   $\text{PO}_4^{3-}$  ( $420 \text{ cm}^{-1}$ ),  $\nu_3$   $\text{PO}_4^{3-}$  ( $1037 \text{ cm}^{-1}$ ),  $\nu_4$   $\text{PO}_4^{3-}$  ( $580 \text{ cm}^{-1}$ ),  $\nu_1$   $\text{HPO}_4^{2-}$  ( $1007 \text{ cm}^{-1}$ ), and  $\nu_1$   $\text{CO}_3^{2-}$  (B type,  $1073 \text{ cm}^{-1}$ ; A type,  $1111 \text{ cm}^{-1}$ ) bands were ascribed to the inorganic phase, while the amide I ( $1672 \text{ cm}^{-1}$ ), amide III ( $1247 \text{ cm}^{-1}$ ), and C–H bending ( $1452 \text{ cm}^{-1}$ ) bands were attributed to the organic phase (Figure 2D). The areas of amide I and C–H bending peaks were associated with the content of organic component, while the area of  $\nu_1$   $\text{PO}_4^{3-}$  was related to the content of inorganic component. There was no significant difference in the areas of amide I and  $\nu_1$   $\text{PO}_4^{3-}$  bands between three dentin layers evaluated, which indicated that the content of organic and inorganic component did not introduce effect to the mechanical characteristics of pseudoosteodentine (Table 1).

The band corresponding to the  $\nu_1$   $\text{PO}_4^{3-}$  symmetric stretching vibration was usually the most intense feature of calcium (Ca) phosphate and apatite spectra,<sup>22</sup> and this band was also evident in the spectra of orthodontine and osteodentine in our study. In the case of HA, the crystallinity was usually estimated from the reciprocal of the FWHM of the  $\nu_1$   $\text{PO}_4^{3-}$  band.<sup>18</sup> In general, the narrower the spectral peak width, the higher the degree of mineral crystallinity.<sup>21</sup> The FWHM of the  $\nu_1$   $\text{PO}_4^{3-}$  band was  $15.4 \text{ cm}^{-1}$  for outer orthodontine of *T. lepturus*,  $17.6 \text{ cm}^{-1}$  for middle osteodentine,

**Table 1. Area of  $\nu_1$   $\text{PO}_4^{3-}$  Peak at  $963\text{ cm}^{-1}$  and the amid-I at  $1672\text{ cm}^{-1}$  from the Outer Orthodontine to the Inner Osteodontine<sup>a</sup>**

area	outer layer(or)	middle layer(os)	inner layer(os)
$\nu_1$ $\text{PO}_4^{3-}$	15,303 $\pm$ 511.4	17,012 $\pm$ 1280	17,549 $\pm$ 3003
amid-I	5087 $\pm$ 1866	5937 $\pm$ 1223	4323 $\pm$ 904.6

<sup>a</sup>or, orthodontine; os, osteodontine. Note: table entries were mean  $\pm$  standard deviation.

and  $18.3\text{ cm}^{-1}$  for inner osteodontine (Figure 2E). In conclusion, applying spectral features between 200 and  $3200\text{ cm}^{-1}$  allowed the distinguishing of the compositions and crystallinity of the pseudoosteodontine of *T. lepturus*. Plenty of studies have demonstrated that crystallinity positively correlated with crystal size.<sup>23</sup> In agreement with their claim, our Raman analysis indirectly confirmed the SEM ultrastructure observations (Figure 2A–C).

**3.3. Mechanical Properties of Pseudoosteodontine of *Trichiurus lepturus*.** Nanoindentation test was used to measure the nano-hardness (indentation hardness [HIT] and Vickers indentation hardness [HVIT]) and nano-stiffness (elastic modulus [E] and indentation modulus [EIT]) of the pseudoosteodontine from outer orthodontine to inner osteodontine (Table 2; Figure 3A–D). The average nano-

**Table 2. Indentation Hardness (HIT), the Indentation Vickers Hardnesses (HV), the Elastic Modulus (E), and the Indentation Elastic Modulus (EIT) Obtained by Nanoindentation for the Pseudoosteodontine of *Trichiurus lepturus* Teeth<sup>a</sup>**

nanoindentation	outer layer(or)	middle layer(os)	inner layer(os)
HIT (GPa)	1.04 $\pm$ 0.08	0.82 $\pm$ 0.09	0.77 $\pm$ 0.07
HVIT (Vickers)	96.34 $\pm$ 7.67	75.66 $\pm$ 7.98	71.75 $\pm$ 6.57
E (GPa)	42.27 $\pm$ 4.74	36.87 $\pm$ 3.75	33.28 $\pm$ 3.84
EIT (GPa)	38.47 $\pm$ 4.32	33.55 $\pm$ 3.41	30.28 $\pm$ 3.5

<sup>a</sup>or, orthodontine; os, osteodontine. Note: table entries were mean  $\pm$  standard deviation.

hardness and nano-stiffness of outer orthodontine were significantly greater than those of middle osteodontine and inner osteodontine, and there were statistical differences between orthodontine and osteodontine. The hardness and stiffness of the middle osteodontine were higher than those of the inner osteodontine, but only the stiffness showed statistical difference. The nano-hardness and nano-stiffness values of pseudoosteodontine positively correlated with its crystalline nanoparticle size (Figure 3E,F). In other words, the larger the pseudoosteodontine crystal particles observed by SEM, the greater the hardness and stiffness.

**3.4. Chemical Elements of Pseudoosteodontine of *Trichiurus lepturus*.** Elemental analysis of transverse sections using EDS revealed that the pseudoosteodontine were comprised mainly of calcium phosphate (Figure 4). Mapping images showed the distributions of carbon (C), phosphorus (P), and calcium (Ca) were relatively uniform throughout the whole pseudoosteodontine of *T. lepturus* (Figure 4B–E). It was worth noting that the magnesium (Mg) content increased seemingly from the outside to the inside (Figure 4C). Therefore, we further carried out EDS quantitative point measurement for the elements of interest in each layer. The mineral compositions of pseudoosteodontine were listed in

Table 3. The outer orthodontine layer had the lowest Mg concentration, followed by the middle and inner layers of osteodontine (Figure 4G). The data showed no differences of C, P as well as Ca/P (Figure 4I,J,L). The Mg concentration appeared to inversely correlate with the concentration of Ca (Figure 4K), suggesting that  $\text{Mg}^{2+}$  and  $\text{Ca}^{2+}$  may be exchangeable within the dentin, which may be relevant to previous reports that replacement of  $\text{Ca}^{2+}$  with  $\text{Mg}^{2+}$  inhibits HA crystal growth.<sup>24</sup> Finally, we found an inverse relationship between the crystalline particle size of the pseudoosteodontine and its Mg concentration, suggesting that  $\text{Mg}^{2+}$  interfered with the crystal maturity (Figure 4H).

## 4. DISCUSSION

In the process of long-term evolution and natural selection, biological organisms ingeniously create high-performance biomaterials from a rather limited number of elements and compounds;<sup>25–27</sup> many even surpass their artificial counterparts.<sup>28,29</sup> Translating the design principles of natural materials into synthetic materials provides a series of feasible ways to obtain unprecedented properties and functions, which are conducive to practical applications in various engineering and medical fields. This strategy fundamentally relies on clarifying the detailed chemical/structural factors, understanding the composition/structure–property relationship, and further extracting the underlying design principles. As a consequence, the correlation between the structure, chemical composition, and mechanical properties of biomaterials has recently become an active research field that aims to develop new biomimetic materials and guide biomimetic mineralization treatments for dental hard tissue diseases.<sup>18,30,31</sup>

Orthodontine is the main type of dentin widely distributed in vertebrates, and osteodontine as a special dentin is only found in chondroid fishes and some teleost fishes.<sup>32</sup> When the tooth has both the orthodontine shell and the osteodontine core, the dentin is called pseudoosteodontine, which has been discovered in recent years.<sup>33</sup> The comparative analysis on the mechanical properties of these two kinds of dentins is only found in the study of the sand tiger shark, *Carcharias Taurus*, and the bonnethead, *Sphyrna tiburo*. The hardness and stiffness of osteodontine from *C. taurus*, are higher than those of orthodontine from *S. tiburo*.<sup>34</sup> Variations in chemical composition are thought to lead to mechanical differences between the two types of dentins. Osteodontine in *C. taurus* contains more Ca than orthodontine in *S. tiburo*, while orthodontine contains more P, Mg, and Na. In addition, the nano-hardness of human enamel is also dependent on Ca and mineral concentrations, so increases in Ca and P concentrations leads to an increase in hardness.<sup>15,35</sup> However, Figure 4 reveals the local concentrations of Ca, P, and the Ca/P ratio do not change significantly from outer orthodontine to inner osteodontine in the teeth of *Trichiurus lepturus*.

HA in teeth is a composition that differs slightly from the usual  $\text{Ca}_5(\text{PO}_4)_3\text{OH}$  stoichiometry and often incorporates impurities, for example,  $\text{Na}^+$ ,  $\text{Mg}^{2+}$ ,  $\text{K}^+$ , and  $\text{Sr}^{2+}$  substitute  $\text{Ca}^{2+}$  cations,  $\text{F}^-$  and  $\text{CO}_3^{2-}$  replace  $\text{PO}_4^{3-}$  or  $\text{OH}^-$  anions.<sup>24</sup> Such element substitutions can change the crystal structure and mechanical properties. For instance, substitution of  $\text{CO}_3^{2-}$  for  $\text{PO}_4^{3-}$  affects physical properties, including micro-crystallite size.<sup>36</sup> When  $[\text{CO}_3^{2-}] \geq 6.5\text{ wt } \%$ , such that nearly every cell contains one  $\text{CO}_3^{2-}$  ion, the crystallinity of minerals is significantly altered.<sup>37</sup> Fluoride can promote crystal maturation and make teeth more resistant to acid attack.<sup>38,39</sup> An increase

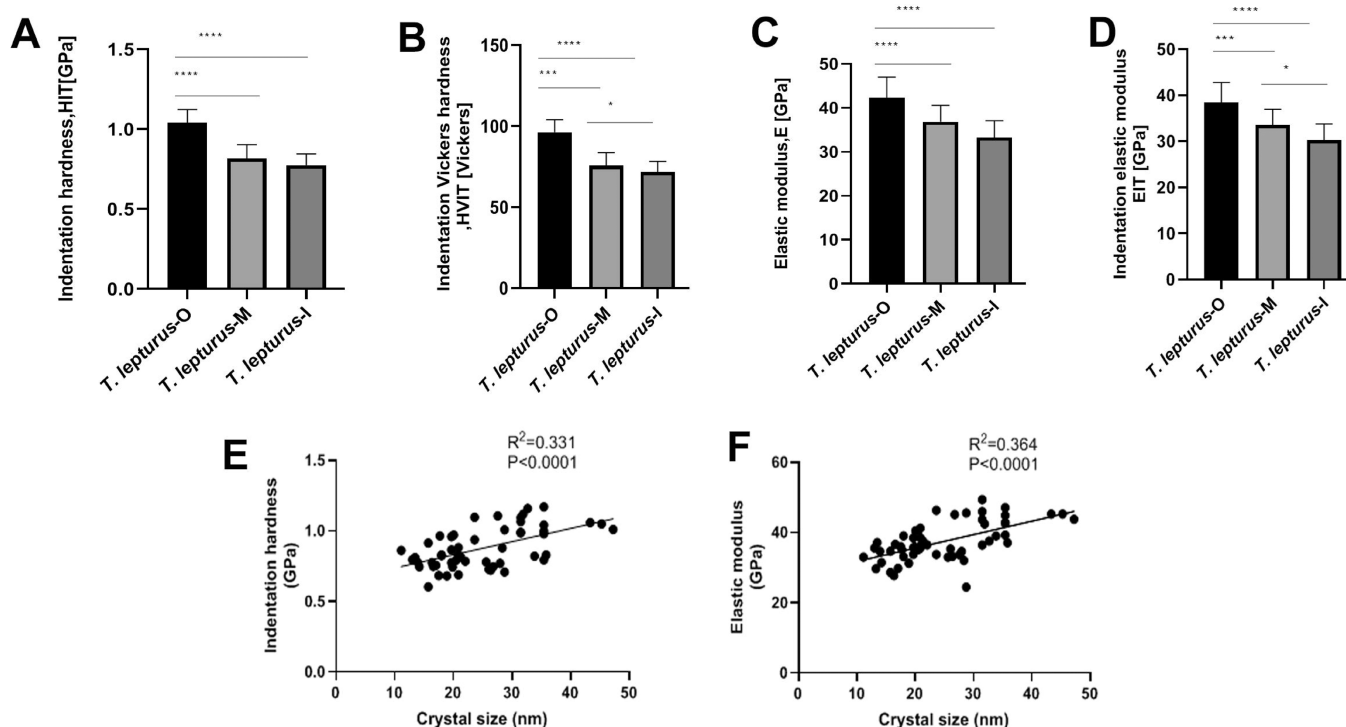


**Figure 3.** Nano-hardness and nano-stiffness of pseudoosteodentine of *Trichiurus lepturus*. (A) Indentation hardness (HIT). (B) Vickers indentation hardness. (C) Elastic modulus. (D) Indentation elastic modulus. (E) Relationship between indentation hardness and crystal size. (F) Correlation between elastic modulus and crystal size. *T. lepturus*-O, outer layer of orthodentine; *T. lepturus*-M, middle layer of osteodentine; and *T. lepturus*-I, inner layer of osteodentine. \* $p < 0.05$ ; \*\* $p < 0.01$ ; \*\*\* $p < 0.001$ ; \*\*\*\* $p < 0.0001$ .

in F, Zn, or Fe results in an accompanying increase in the stiffness and hardness of enamel.<sup>39–41</sup> Magnesium is distributed in an intergranular phase at the grain boundaries of human and rodent enamel and regulates HA crystallization by stabilizing its precursor, amorphous calcium phosphate.<sup>39,42</sup> Substitution of  $Mg^{2+}$  for  $Ca^{2+}$  produces a contraction of the *a*-axis in synthetic HA and reduces the crystal size.<sup>5,43</sup> Magnesium is an inhibitor of mineral growth in solutions containing  $Ca^{2+}$ , phosphate, and apatite crystal seeds.<sup>38</sup> Similarly, our SEM and EDS analyses show that the Mg concentration in pseudoosteodentine of *T. lepturus* is inversely proportional to crystal size. Compared with inner osteodentine, outer orthodentine had larger nanoparticles and lower Mg concentration in our study (Figure 5).

Magnesium ions react with human permanent enamel through the process of dissolution and reprecipitation, which reduces the enamel crystal size on the surface of teeth and makes them harder and whiter.<sup>44</sup> In the same way, treatment of the outer surface of healthy primary molars with magnesium chloride solution was shown to increase the nano-hardness of enamel by approximately 20%.<sup>13</sup> On the contrary, Cuy et al. found that the concentration of Mg in enamel increased commensurately with the distance from the outer surface to the enamel–dentin junction, whereas the hardness simultaneously decreased.<sup>15</sup> Elemental analysis of the human enamel–dental junction shows that the Mg concentration in enamel is significantly lower than that in dentin, which may explain why the crystal size in dentin is smaller than that in enamel. The hardness of dentin is lower than that of enamel.<sup>45</sup> Other studies have similarly found that the  $Mg^{2+}$  concentration increases from the enamel surface to the dentin–enamel junction.<sup>46</sup> In line with the later studies, we found that the

$Mg^{2+}$  concentration increases gradually from outer orthodentine to inner osteodentine, while the nano-hardness decreases gradually. Magnesium is normally removed from the enamel crystal space to allow mineralization to occur, and an increased Mg concentration impairs crystal growth and maturation.<sup>47</sup> The phenomenon we found might be explained by this theory.

In addition to the chemical composition, the structural features, such as the dimension and distribution can affect the mechanical properties of biomaterials. Boskey hypothesized that the crystal size and perfection of bone mineral influence mechanical strength. This hypothesis is supported by the observation that bone composites containing only large crystals or only small crystals are mechanically weaker than those with a broad distribution of crystal sizes. The bones of younger animals are stronger and composed of a mixture of small newly formed and large mature crystals. A broad distribution of crystal sizes may enhance resistance to load.<sup>9</sup> Our high-resolution SEM images reveal similar conditions in pseudoosteodentine of *T. lepturus*. A multitude of composite particles mixed with large and small crystals, are predominantly distributed in the outer orthodentine layer, whereas the inner osteodentine layer is relatively rich in uniform small crystals; by contrast, the middle osteodentine layer exhibits an intermediate distribution of larger composite and smaller crystals. The expanded distribution of crystal size may promote both nano-hardness and nano-stiffness of the outer orthodentine in this study.

Many functions and properties of biomaterials are largely determined by the size of their components, which is reminiscent of the well-known Hall–Petch relationship in crystals. This provides a feasible method for developing gradients by altering the characteristic structural size of these

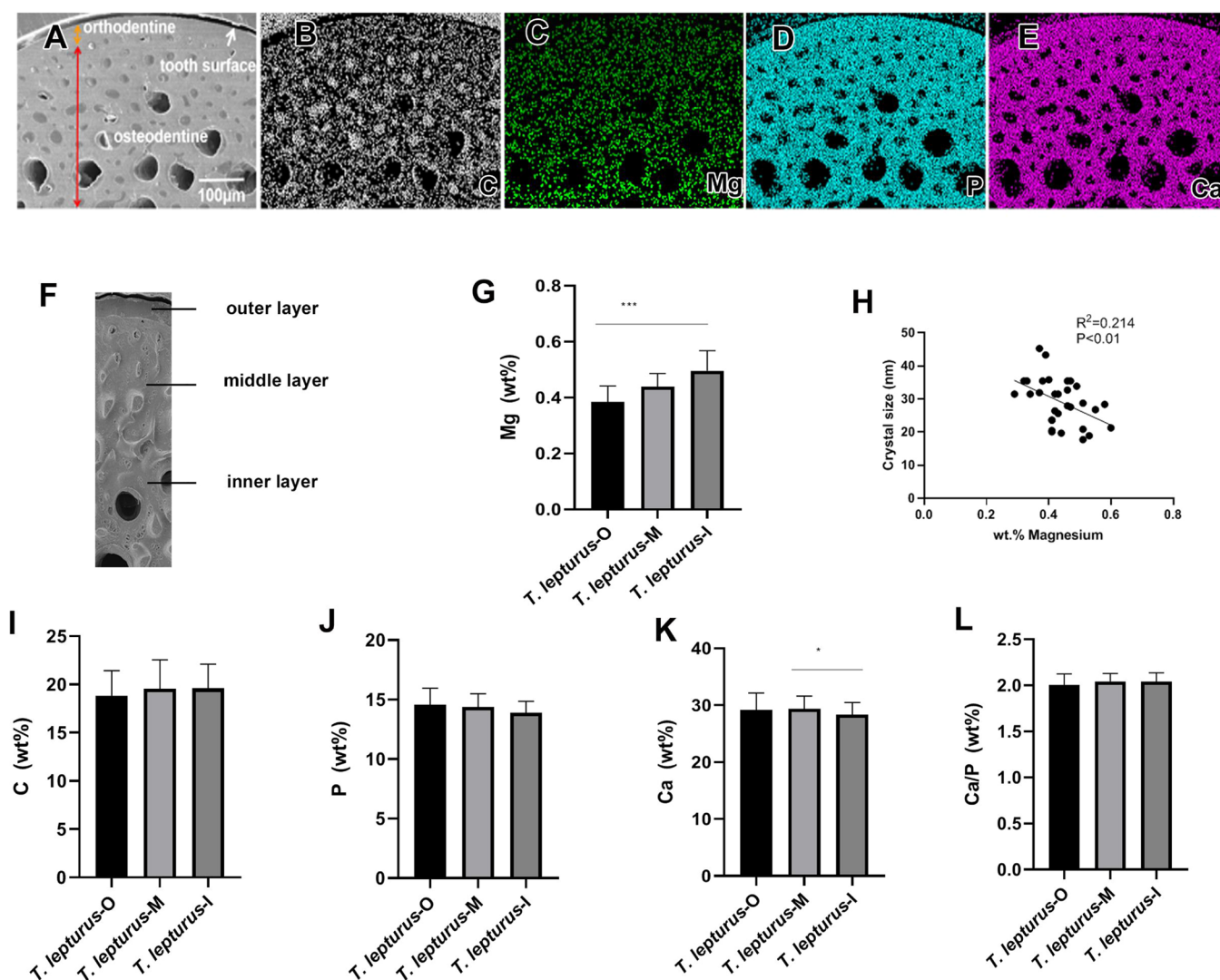


**Figure 4.** Distribution and concentration of chemical elements obtained by EDS microanalysis of the pseudoosteodentine of *Trichiurus lepturus*. (A) SEM image of the pseudoosteodentine of a transverse section from outer orthodentine to inner osteodentine. (B–E) Distribution of carbon (C), magnesium (Mg), phosphorus (P), and calcium (Ca). (F) The locations of a cross section marked with straight lines are used for point elemental analysis. (G) Comparison of Mg content. (H) The negative relationship between Mg content (wt %) and crystalline particle size of pseudoosteodentine. Fifty-nine indents were conducted on the sample. (I and L) Comparison of C, P content, Ca content, and the Ca/P ratio. *T. lepturus-O*, outer layer of orthodentine; *T. lepturus-M*, middle layer of osteodentine; and *T. lepturus-I*, inner layer of osteodentine. \* $p < 0.05$ ; \*\* $p < 0.01$ ; \*\*\* $p < 0.001$ ; \*\*\*\* $p < 0.0001$ .

**Table 3. Chemical Elements Content of the Pseudoosteodentine in *Trichiurus lepturus* Teeth<sup>a</sup>**

element	outer layer(or)	middle layer(os)	inner layer(os)
C (wt %)	18.81 ± 2.63	19.54 ± 3.01	19.59 ± 2.50
Na (wt %)	0.36 ± 0.24	0.19 ± 0.23	0.14 ± 0.21
Mg (wt %)	0.38 ± 0.06	0.44 ± 0.05	0.49 ± 0.07
P (wt%)	14.55 ± 1.40	14.40 ± 1.10	13.90 ± 0.96
Ca (wt%)	29.15 ± 3.01	29.39 ± 2.23	28.36 ± 2.13
Ca/P	2.01 ± 0.12	2.04 ± 0.09	2.04 ± 0.10

<sup>a</sup>or, orthodentine; os, osteodentine. Note: table entries were mean ± standard deviation.

materials. According to the Hall–Petch relation, hardness is greatly increased by refining the size of the crystal.<sup>48,49</sup> For example, the crystals size of HA along the *c*-axis increases from the buccal surface to the deep layer in the enamel of the human incisors and canines. Such a variation results in graded

mechanical properties across the tissue with the buccal surface being harder than the deep layer.<sup>50</sup> It should be noted that some materials compose of nanocrystals do not follow this law, and hardness positively correlates with crystal size if the crystals are smaller than the critical size.<sup>51</sup> Another study using third molar enamel as a graded biomaterial shows the crystallite size and crystallinity of HA decreases from the enamel surface to the enamel–dentin junction, leading to obvious mechanical gradients of decreasing hardness along the opposite direction.<sup>52</sup> Likewise, from superficial dentin to deep dentin, the micro-hardness of third molar dentin exhibits decreasing trend and is positively correlated with HA crystallinity.<sup>53</sup> The crystallinity is usually proportional to the crystal size.<sup>23</sup> Enamel contains parallel crystals approximately 50 nm wide and several microns long,<sup>4</sup> while HA crystals in dentin are flat, 60~70 nm long, 20~30 nm wide, and 3~4 nm thick by transmission electron microscope. In our study, the crystal size of the pseudoosteodentine in the teeth of *T.*

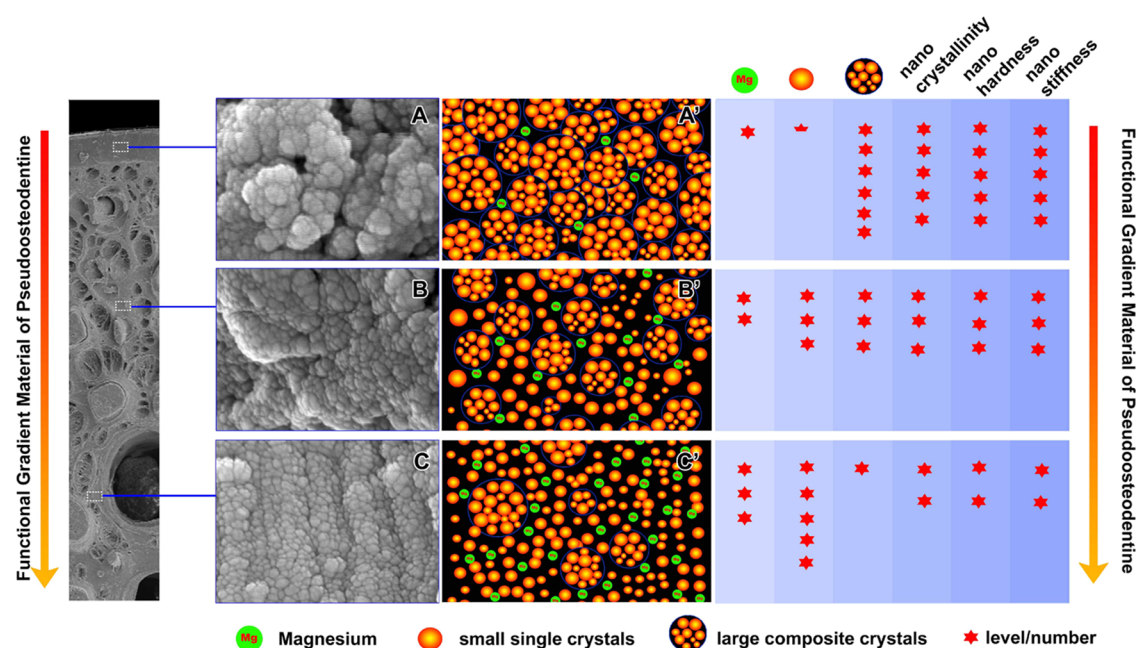


**Figure 5.** Gradient change of pseudoosteodentine as derived from teeth of *Trichiurus lepturus*, based on Mg content, crystal size, crystallinity, nano-hardness, and nano-stiffness. Scanning electron micrograph at low magnification of embedded and etched *T. lepturus* tooth showed the SEM at high magnification were acquired on the three square regions (none etched) of outer, middle, and inner pseudoosteodentine, respectively. (A–A') Scanning electron micrograph and schematic model of outer pseudoosteodentine (orthodontine). (B–B') Scanning electron micrograph and schematic model of middle pseudoosteodentine (osteodentine). (C–C') Scanning electron micrograph and schematic model of inner pseudoosteodentine (osteodentine).

*lepturus* is approximate 17~33 nm, which we speculate to be smaller than the critical size. Consequently, the pseudoosteodentine no longer follows Hall–Petch law, but the crystal size decreases from the outer orthodontine layer to the inner osteodentine layer, resulting in a concurrent decrease in crystallinity and nano-hardness.

The crystallinity and crystal size of HA is highest at the outer orthodontine and decreases gradually toward the inner osteodentine, which are influenced by the increasing content of magnesium in the teeth of *T. lepturus*, as shown above. As a result, the local nano-hardness exhibits a concomitant decrease, from 0.77 to 1.04 GPa, along the radial direction, representing characteristic features of so called functional gradient materials (FGMs). The term "gradient" is widely used to describe the nonuniformity of materials, often near surface or internal interface, in contrast to strict uniformity; it also involves a gradual transition between different nano-/microstructure rather than a sudden change. It has been known for some time that the application of spatial gradients can effectively enhance the mechanical and functional performance of materials, for example, alleviating singularities or stress concentrations, improving interfacial bonding, and enabling new functions.<sup>54–57</sup> Functional gradients have been identified as a basic structural element in nature<sup>58</sup> and is widely used in biomaterials with various structures.<sup>25,59,60</sup> These gradients have effectively realized their functions under specific environmental constraints. Therefore, they represent an ideal paradigm from which meaningful guidelines for synthetic materials can be derived. These gradients are essentially related with the graded changes of local chemical constituents and structural characteristics involved in the arrangement, distribution, dimensions, and orientations of the building blocks. In addition to the chemical composition and crystal structure of pseudoosteodentine discussed above, akin to graded

antler,<sup>61</sup> the pore and tubule structure can also affect the overall performance of the material. In our SEM images, the porosity increases continuously with the transition from outer compact orthodontine to inner lacunaris osteodentine. This pattern represents a common design form in nature, with a porous core supporting a dense periphery with high bending stiffness.<sup>28,29</sup> The outer orthodontine layer is harder and has a good resistance to direct external loads, while the poriferous internal osteodentine can enable energy dissipation; together, these properties may enable pseudoosteodentine of *T. lepturus* to withstand large stresses. Of course, since the indentation size (radius = 100 nm) and indentation depth (280 nm) are smaller than the width of the dentinal osteons (10–65  $\mu\text{m}$ ), the mechanical differences between the two dentin in our current study do not derive from the distribution of pores.

## 5. CONCLUSIONS

The morphology, microstructure, chemical composition, and mechanical properties of *Trichiurus lepturus* dentin were analyzed in detail using micro-CT, SEM, EDS, Raman spectroscopy, and nanoindentation. We showed that *T. lepturus* dentin is a special type of pseudoosteodentine among vertebrates. The outer compact orthodontine is characterized by parallel dentin tubules and covers the porous osteodentine that replaces the dental pulp cavity. Both orthodontine and osteodentine are composed of oval-shaped HA nanocrystals, which have no abrupt interface. Although there is no significant difference in the concentrations of C, P, Ca, and Ca/P, the Mg concentration in the outer orthodontine layer is lower than that in the inner layers of osteodentine. Magnesium is essential for the normal development of tooth structure, but its role in biomineralization is unclear. In this study, we showed that larger local concentrations of Mg are associated with smaller crystal sizes and less crystallinity, and that the hardness of the

inner osteodentine layer is lower than that of the outer orthodentine layers. The physicochemical properties of pseudoosteodentine of *T. lepturus* change gradually throughout the tooth. The harder orthodentine provides a protective shell, while the flexible osteodentine acts as an elastic substrate. Therefore, as an FGM, pseudoosteodentine of *T. lepturus* provides a solid foundation for the bionic design of dental materials.

## AUTHOR INFORMATION

### Corresponding Author

**Xiaofeng Huang** – Department of Stomatology and Immunology Research Center for Oral and Systemic Health, Beijing Friendship Hospital, Capital Medical University, Beijing 100050, China; [orcid.org/0000-0002-2082-5742](https://orcid.org/0000-0002-2082-5742); Phone: 086 010 63138415; Email: [xiaofengh@ccmu.edu.cn](mailto:xiaofengh@ccmu.edu.cn), [huangxf1998@163.com](mailto:huangxf1998@163.com); Fax: 086 010 63038519

### Authors

**Li Tang** – Department of Stomatology and Immunology Research Center for Oral and Systemic Health, Beijing Friendship Hospital, Capital Medical University, Beijing 100050, China; Department of Orthodontics, The Affiliated Hospital of Qingdao University, Qingdao 266005, China; School of Stomatology, Qingdao University, Qingdao 266071, China

**Yongfeng Li** – Department of Stomatology and Immunology Research Center for Oral and Systemic Health, Beijing Friendship Hospital, Capital Medical University, Beijing 100050, China

**Ruiqi Li** – Department of Stomatology and Immunology Research Center for Oral and Systemic Health, Beijing Friendship Hospital, Capital Medical University, Beijing 100050, China

**Xingfu Tao** – National Institute of Metrology, Beijing 100013, China

Complete contact information is available at:

<https://pubs.acs.org/10.1021/acsomega.2c04808>

### Notes

The authors declare no competing financial interest.

## ACKNOWLEDGMENTS

This work was supported by grants awarded by the National Natural Science Foundation of China (No. 82071141) and the Natural Science Foundation of Beijing Municipality (No. 7202036) to X.H.

## REFERENCES

- (1) Moyer, J. K.; Bemis, W. E. Shark teeth as edged weapons: serrated teeth of three species of selachians. *Zoology (Jena)* **2017**, *120*, 101–109.
- (2) Berthaume, M. A.; Lazzari, V.; Guy, F. The landscape of tooth shape: Over 20 years of dental topography in primates. *Evol. Anthropol.* **2020**, *29*, 245–262.
- (3) Solaymani, S.; Nezafat, N. B.; Tãlu, Ş.; Shafiekhani, A.; Dalouji, V.; Amiri, A.; Rezaee, S.; Morozov, I. A. Atomic force microscopy studies of enamel, inner enamel, dentin, and cementum in canine teeth. *Microsc. Res. Tech.* **2021**, *84*, 1098–1105.
- (4) Beniash, E.; Stiffler, C. A.; Sun, C. Y.; Jung, G. S.; Qin, Z.; Buehler, M. J.; Gilbert, P. The hidden structure of human enamel. *Nat. Commun.* **2019**, *10*, 4383.

- (5) Ortiz-Ruiz, A. J.; Teruel-Fernández, J. D.; Alcolea-Rubio, L. A.; Hernández-Fernández, A.; Martínez-Beneyto, Y.; Gispert-Guirado, F. Structural differences in enamel and dentin in human, bovine, porcine, and ovine teeth. *Ann. Anat.* **2018**, *218*, 7–17.

- (6) Roschger, A.; Wagermaier, W.; Gamsjaeger, S.; Hassler, N.; Schmidt, I.; Blouin, S.; Berzlanovich, A.; Gruber, G. M.; Weinkamer, R.; Roschger, P.; Paschalis, E. P.; Klaushofer, K.; Fratzl, P. Newly formed and remodeled human bone exhibits differences in the mineralization process. *Acta Biomater.* **2020**, *104*, 221–230.

- (7) Jambura, P. L.; Türtscher, J.; Kindlimann, R.; Metscher, B.; Pfaff, C.; Stumpf, S.; Weber, G. W.; Kriwet, J. Evolutionary trajectories of tooth histology patterns in modern sharks (Chondrichthyes, Elasmobranchii). *J. Anat.* **2020**, *236*, 753–771.

- (8) Arola, D. D.; Gao, S.; Zhang, H.; Masri, R. The Tooth: Its Structure and Properties. *Dent. Clin. North Am.* **2017**, *61*, 651–668.

- (9) Boskey, A. Bone mineral crystal size. *Osteoporos. Int.* **2003**, *14*, S16–S20.

- (10) Wingender, B.; Azuma, M.; Krywka, C.; Zaslansky, P.; Boyle, J.; Deymier, A. Carbonate substitution significantly affects the structure and mechanics of carbonated apatites. *Acta Biomater.* **2021**, *122*, 377–386.

- (11) Qamar, Z.; Haji Abdul Rahim, Z. B.; Chew, H. P.; Fatima, T. Influence of trace elements on dental enamel properties: A review. *J. Pak. Med. Assoc.* **2017**, *67*, 116–120.

- (12) Erem, S.; Atfi, A.; Razzaque, M. S. Anabolic effects of vitamin D and magnesium in aging bone. *J. Steroid Biochem. Mol. Biol.* **2019**, *193*, No. 105400.

- (13) Kis, V. K.; Sulyok, A.; Hegedűs, M.; Kovács, I.; Rózsa, N.; Kovács, Z. Magnesium incorporation into primary dental enamel and its effect on mechanical properties. *Acta Biomater.* **2021**, *120*, 104–115.

- (14) Halusic, A. M.; Sepich, V. R.; Shirley, D. C.; Granjeiro, J. M.; Costa, M. C.; Kuchler, E. C.; Vieira, A. R. Calcium and magnesium levels in primary tooth enamel and genetic variation in enamel formation genes. *Pediatr. Dent.* **2014**, *36*, 384–388.

- (15) Cuy, J. L.; Mann, A. B.; Livi, K. J.; Teaford, M. F.; Weihs, T. P. Nanoindentation mapping of the mechanical properties of human molar tooth enamel. *Arch. Oral Biol.* **2002**, *47*, 281–291.

- (16) Tang, L.; Li, Y. F.; Li, R. Q.; Zhang, M. Y.; Huang, X. F. Development and structural characteristics of pseudoosteodentine in the Pacific cutlassfish. *Trichiurus lepturus*. *Tissue Cell* **2022**, *77*, No. 101847.

- (17) Moradian-Oldak, J.; George, A. Biomineralization of Enamel and Dentin Mediated by Matrix Proteins. *J. Dent. Res.* **2021**, *100*, 1020–1029.

- (18) Guentsch, A.; Fahmy, M. D.; Wehrle, C.; Nietzsche, S.; Popp, J.; Watts, D. C.; Kranz, S.; Krafft, C.; Sigusch, B. W. Effect of biomimetic mineralization on enamel and dentin: A Raman and EDX analysis. *Dent. Mater.* **2019**, *35*, 1300–1307.

- (19) Oliver, W. C.; Pharr, G. M. An improved technique for determining hardness and elastic modulus using load and displacement sensing indentation experiments. *J. Mater. Res.* **1992**, *7*, 1564–1583.

- (20) Ramakrishnaiah, R.; Rehman, G. U.; Basavarajappa, S.; Khuraif, A. A. A.; Durgesh, B. H.; Khan, A. S.; Rehman, I. U. Applications of Raman Spectroscopy in Dentistry: Analysis of Tooth Structure. *Appl. Spectrosc. Rev.* **2015**, *50*, 332–350.

- (21) Shah, F. A. Towards refining Raman spectroscopy-based assessment of bone composition. *Sci. Rep.* **2020**, *10*, 16662.

- (22) Pasteris, J. D.; Wopenka, B.; Freeman, J. J.; Rogers, K.; Valsami-Jones, E.; van der Houwen, J. A.; Silva, M. J. Lack of OH in nanocrystalline apatite as a function of degree of atomic order: implications for bone and biomaterials. *Biomaterials* **2004**, *25*, 229–238.

- (23) Reyes-Gasga, J.; Martinez-Pineiro, E. L.; Rodriguez-Alvarez, G.; Tiznado-Orozco, G. E.; Garcia-Garcia, R.; Bres, E. F. XRD and FTIR crystallinity indices in sound human tooth enamel and synthetic hydroxyapatite. *Mater. Sci. Eng., C* **2013**, *33*, 4568–4574.

- (24) Teruel Jde, D.; Alcolea, A.; Hernández, A.; Ruiz, A. J. Comparison of chemical composition of enamel and dentine in human, bovine, porcine and ovine teeth. *Arch. Oral Biol.* **2015**, *60*, 768–775.
- (25) Amini, S.; Masic, A.; Bertinetti, L.; Teguh, J. S.; Herrin, J. S.; Zhu, X.; Su, H.; Miserez, A. Textured fluorapatite bonded to calcium sulphate strengthen stomatopod raptorial appendages. *Nat. Commun.* **2014**, *5*, 3187.
- (26) Politi, Y.; Priewasser, M.; Pippel, E.; Zaslansky, P.; Hartmann, J.; Siegel, S.; Li, C.; Barth, F. G.; Fratzl, P. A Spider's Fang: How to Design an Injection Needle Using Chitin-Based Composite Material. *Adv. Funct. Mater.* **2012**, *22*, 2519–2528.
- (27) Chen, P. Y.; Lin, A. Y.; Lin, Y. S.; Seki, Y.; Stokes, A. G.; Peyras, J.; Olevisky, E. A.; Meyers, M. A.; McKittrick, J. Structure and mechanical properties of selected biological materials. *J. Mech. Behav. Biomed. Mater.* **2008**, *1*, 208–226.
- (28) Chen, P. Y.; Mckittrick, J.; Meyers, M. A. Biological materials: Functional adaptations and bioinspired designs. *Prog. Mater. Sci.* **2012**, *57*, 1492–1704.
- (29) Meyers, M. A.; McKittrick, J.; Chen, P. Y. Structural biological materials: critical mechanics-materials connections. *Science* **2013**, *339*, 773–779.
- (30) Weng, Z. Y.; Liu, Z. Q.; Ritchie, R. O.; Jiao, D.; Li, D. S.; Wu, H. L.; Deng, L. H.; Zhang, Z. F. Giant panda's tooth enamel: Structure, mechanical behavior and toughening mechanisms under indentation. *J. Mech. Behav. Biomed. Mater.* **2016**, *64*, 125–138.
- (31) Enax, J.; Janus, A. M.; Raabe, D.; Eppel, M.; Fabritius, H. O. Ultrastructural organization and micromechanical properties of shark tooth enameloid. *Acta Biomater.* **2014**, *10*, 3959–3968.
- (32) Huyseune, A.; Sire, J. Y. Evolution of patterns and processes in teeth and tooth-related tissues in non-mammalian vertebrates. *Eur. J. Oral Sci.* **1998**, *106*, 437–481.
- (33) Jambura, P. L.; Pfaff, C.; Underwood, C. J.; Ward, D. J.; Kriwet, J. Tooth mineralization and histology patterns in extinct and extant snaggletooth sharks, Hemipristis (Carcharhiniformes, Hemigaleidae)-Evolutionary significance or ecological adaptation? *PLoS One* **2018**, *13*, No. e0200951.
- (34) Whitenack, L. B.; Simkins, D. C., Jr.; Motta, P. J.; Hirai, M.; Kumar, A. Young's modulus and hardness of shark tooth biomaterials. *Arch. Oral Biol.* **2010**, *55*, 203–209.
- (35) Jeng, Y. R.; Lin, T. T.; Hsu, H. M.; Chang, H. J.; Shieh, D. B. Human enamel rod presents anisotropic nanotribological properties. *J. Mech. Behav. Biomed. Mater.* **2011**, *4*, 515–522.
- (36) Legeros, R. Z.; Trautz, O. R.; Legeros, J. P.; Klein, E.; Shirra, W. P. Apatite crystallites: effects of carbonate on morphology. *Science* **1967**, *155*, 1409–1411.
- (37) McElderry, J. D.; Zhu, P.; Mroue, K. H.; Xu, J.; Pavan, B.; Fang, M.; Zhao, G.; McNerny, E.; Kohn, D. H.; Franceschi, R. T.; Holl, M. M.; Tecklenburg, M. M.; Ramamoorthy, A.; Morris, M. D. Crystallinity and compositional changes in carbonated apatites: Evidence from (31)P solid-state NMR, Raman, and AFM analysis. *J. Solid State Chem.* **2013**, *206*, 192–198.
- (38) Okazaki, M.; LeGeros, R. Z. Properties of heterogeneous apatites containing magnesium, fluoride, and carbonate. *Adv. Dent. Res.* **1996**, *10*, 252–259.
- (39) Gordon, L. M.; Cohen, M. J.; MacRenaris, K. W.; Pasteris, J. D.; Seda, T.; Joester, D. Dental materials. Amorphous intergranular phases control the properties of rodent tooth enamel. *Science* **2015**, *347*, 746–750.
- (40) Deang, J. F.; Persons, A. K.; Oppedal, A. L.; Rhee, H.; Moser, R. D.; Horstemeyer, M. F. Structure, property, and function of sheephead (Archosargus probatocephalus) teeth. *Arch. Oral Biol.* **2018**, *89*, 1–8.
- (41) Bentov, S.; Palmer, B. A.; Bar-On, B.; Shelef, Y.; Aflalo, E. D.; Sagi, A. Reinforcement of bio-apatite by zinc substitution in the incisor tooth of a prawn. *Acta Biomater.* **2021**, *120*, 116–123.
- (42) La Fontaine, A.; Zavgorodniy, A.; Liu, H.; Zheng, R.; Swain, M.; Cairney, J. Atomic-scale compositional mapping reveals Mg-rich amorphous calcium phosphate in human dental enamel. *Sci. Adv.* **2016**, *2*, No. e1601145.
- (43) LeGeros, R. Z.; Sakae, T.; Bautista, C.; Retino, M.; LeGeros, J. P. Magnesium and carbonate in enamel and synthetic apatites. *Adv. Dent. Res.* **1996**, *10*, 225–231.
- (44) Abdallah, M. N.; Eimar, H.; Bassett, D. C.; Schnabel, M.; Ciobanu, O.; Nelea, V.; McKee, M. D.; Cerruti, M.; Tamimi, F. Diagenesis-inspired reaction of magnesium ions with surface enamel mineral modifies properties of human teeth. *Acta Biomater.* **2016**, *37*, 174–183.
- (45) Wang, R.; Zhao, D.; Wang, Y. Characterization of elemental distribution across human dentin-enamel junction by scanning electron microscopy with energy-dispersive X-ray spectroscopy. *Microsc. Res. Tech.* **2021**, *84*, 881–890.
- (46) Robinson, C.; Shore, R. C.; Brookes, S. J.; Strafford, S.; Wood, S. R.; Kirkham, J. The chemistry of enamel caries. *Crit. Rev. Oral Biol. Med.* **2000**, *11*, 481–495.
- (47) Bronckers, A. L.; Lyaruu, D. M. Magnesium, pH regulation and modulation by mouse ameloblasts exposed to fluoride. *Bone* **2017**, *94*, 56–64.
- (48) Tipper, C. F.; Barr, W.; Thring, M. W.; Hundy, B. B.; Petch, N. J. Effect of direction of rolling, direction of straining, and ageing on the mechanical properties of a mild steel plate-discussion. *J. Iron Steel Res. Int.* **1953**, *173*, 280–284.
- (49) Hall, E. O. The Deformation and Ageing of Mild Steel: III Discussion of Results. *Proc. Phys. Soc. B* **1951**, *64*, 742.
- (50) Eimar, H.; Ghadimi, E.; Marelli, B.; Vali, H.; Nazhat, S. N.; Amin, W. M.; Torres, J.; Ciobanu, O.; Junior, R. A.; Tamimi, F. Regulation of enamel hardness by its crystallographic dimensions. *Acta Biomater.* **2012**, *8*, 3400–3410.
- (51) Baldwin, W. M. Yield strength of metals as a function of grain size. *Acta Metall.* **1958**, *6*, 139–141.
- (52) Low, I. M. Depth-Profiling of Crystal Structure, Texture, and Microhardness in a Functionally Graded Tooth Enamel. *J. Am. Ceram. Soc.* **2004**, *87*, 2125–2131.
- (53) Seyedmahmoud, R.; McGuire, J. D.; Wang, Y.; Thiagarajan, G.; Walker, M. P. The interrelationship of microstructure and hardness of human coronal dentin using reference point indentation technique and micro-Raman spectroscopy. *Dent. Mater.* **2017**, *33*, 1069–1074.
- (54) Sola, A.; Bellucci, D.; Cannillo, V. Functionally graded materials for orthopedic applications - an update on design and manufacturing. *Biotechnol. Adv.* **2016**, *34*, 504–531.
- (55) Suresh, S. Graded materials for resistance to contact deformation and damage. *Science* **2001**, *292*, 2447–2451.
- (56) Fang, T. H.; Li, W. L.; Tao, N. R.; Lu, K. Revealing extraordinary intrinsic tensile plasticity in gradient nano-grained copper. *Science* **2011**, *331*, 1587–1590.
- (57) Liu, Z. Q.; Meyers, M. A.; Zhang, Z. F.; Ritchie, R. O. Functional gradients and heterogeneities in biological materials: Design principles, functions, and bioinspired applications. *Prog. Mater. Sci.* **2017**, *88*, 467–498.
- (58) Naleway, S. E.; Porter, M. M.; McKittrick, J.; Meyers, M. A. Structural Design Elements in Biological Materials: Application to Bioinspiration. *Adv. Mater.* **2015**, *27*, 5455–5476.
- (59) Weaver, J. C.; Wang, Q.; Miserez, A.; Tantuccio, A.; Stromberg, R.; Bozhilov, K. N.; Maxwell, P.; Nay, R.; Heier, S. T.; Masi, D. Analysis of an ultra hard magnetic biomineral in chiton radular teeth. *Mater. Today* **2010**, *13*, 42–52.
- (60) Gibson, L. J. The hierarchical structure and mechanics of plant materials. *J. R. Soc., Interface* **2012**, *9*, 2749–2766.
- (61) Chen, P. Y.; Stokes, A. G.; McKittrick, J. Comparison of the structure and mechanical properties of bovine femur bone and antler of the North American elk (*Cervus elaphus canadensis*). *Acta Biomater.* **2009**, *5*, 693–706.